

Article

Selective Hydrogenation of 3-Nitrostyrene over a Co-promoted Pt Catalyst Supported on P-containing Activated Charcoal

Qifan Wu ^{1,2,3}, Chao Zhang ^{1,3,*} , Weiwei Lin ^{1,3}, Haiyang Cheng ^{1,3}, Masahiko Arai ^{1,3} and Fengyu Zhao ^{1,2,3,*}

¹ State Key Laboratory of Electroanalytical Chemistry, Changchun Institute of Applied Chemistry, Chinese Academy of Sciences, Changchun 130022, China; qifanwu@ciac.ac.cn (Q.W.); linwei@ciac.ac.cn (W.L.); hycyl@ciac.ac.cn (H.C.); marai@eng.hokudai.ac.jp (M.A.)

² School of Applied Chemistry and Engineering, University of Science and Technology of China, Hefei 230026, China

³ Laboratory of Green Chemistry and Process, Changchun Institute of Applied Chemistry, Chinese Academy of Sciences, Changchun 130022, China

* Correspondence: czhang@ciac.ac.cn (C.Z.); zhaofy@ciac.ac.cn (F.Z.); Tel.: +86-431-85262410 (F.Z.)

Received: 12 April 2019; Accepted: 28 April 2019; Published: 8 May 2019



Abstract: A series of Co-modified Pt catalysts supported on P-containing activated charcoal were studied for the selective hydrogenation of 3-nitrostyrene (NS) to 3-aminostyrene (AS). The addition of Co decreased the rate of hydrogenation but enhanced the selectivity to AS, being 92% at nearly 100% conversion over an optimized catalyst. The high AS selectivity should result from the configuration of NS adsorption on the catalyst, which occurs preferentially with its -NO₂ group on the Pt-PO_x interface layer over the surface of supported Pt particles. The formation of such a Pt-PO_x area is promoted by the Co additive.

Keywords: selective hydrogenation; 3-nitrostyrene; bimetallic catalysts

1. Introduction

Carbon materials have been utilized in a wide variety of applications owing to high elemental abundance and diverse bonding capability of carbon atoms. The doping of carbon materials with heteroatoms (B, N, O, P, and S) broadens the fields of the application of carbon materials. Heteroatom-doped carbon materials have attracted much attention in the field of heterogeneous catalysis owing to their tunable surface structures and electronic properties [1–12]. The influence of N-doping to carbon materials on their catalytic performance has been extensively studied [13–15]. Synergistic effects of nitrogen atoms in the carbon architecture combined with metal nanoparticles can find application in a wide range of catalytic reactions [16]. In addition, phosphorus (P) has the same number of valence electrons as nitrogen, but bigger atomic radius and better electron-donating ability than nitrogen, which could change local charge density through its lone pair electrons in the 3*p* orbital. Such characters are effective to improve the electronic density of nearby carbon atoms and produce defect sites in P-doped carbon materials [17–20]. Consequently, such surface modifications would lead to a change in the performance of supported catalysts thereon [21–26]. For instance, P-doped carbon materials could promote the dispersion of supported Pt nanoparticles, which is beneficial for improving catalytic activity [26–29]. Moreover, the significant orbital hybridization between the transition metal *sd* hybridized orbital and P *sp* hybridized orbital, changes the electronic structure of the metal, which has positive impacts on the catalytic activity of the metals [7]. The interactions between

P-containing species and the metal active sites could also influence the adsorption configurations of reactants adsorbed on the catalysts [7,17].

Hydrogenation reactions are practically important chemical processes [10,30–35], and, for example, those of aromatic nitro compounds to anilines are widely used for the manufacture of pharmaceuticals, pesticides, fine chemicals, and pigments [36–42]. Although the selective hydrogenation of nitro groups have been widely investigated so far, efforts still need to design more selective catalysts.

Supported PtCo catalysts have been studied in catalytic hydrogenation due to their unique electronic, geometric, and structural properties, and these bimetallic catalysts show excellent catalytic performances in the selective hydrogenation of C=O, C=C, N=O, and others [43–48]. For cinnamaldehyde hydrogenation, for instance, 91% selectivity to cinnamyl alcohol (COL) was obtained on Pt₃Co/Co(OH)₂ catalysts owing to the modified electron density of Pt [49]. A selectivity to COL (>90%) was achieved over Pt–Co/MWCNTs (multi-walled carbon nanotubes), which was attributed to the synergistic effect between Pt–Co and MWCNTs [43]. Thus, Co can be an interesting additive and modifier to change the catalytic performances of supported Pt catalysts. Recently the authors have found that the selectivity of carbon-supported Pt catalyst in liquid phase hydrogenation of 3-nitrostyrene (NS) can be switched by the modification of the Pt by phosphorous species, from ethylnitrobenzene (ENB)—selective to aminostyrene (AS)—selective. That is, the nitro group of NS is selectively hydrogenated to AS with Pt catalyst supported on P-containing activated charcoal (PAC) compared with the vinyl group [50]. In a Pt/PAC catalyst, Pt–PO_x interfacial layer is formed on the surface of Pt particles and promotes the adsorption of NS with its nitro group. In the present work, after considering above-mentioned interesting impacts of Co on Pt catalysts and our previous results with Pt/PAC, the influence of Co additive to Pt/PAC on the product selectivity in the same hydrogenation has been studied. It is interesting to note that the AS selectivity is further enhanced by the addition of a Co modifier to Pt/PAC. Synergistic roles of Co additive and surface P species in changing the product selectivity have been examined and discussed on the basis of reaction and catalyst characterization results (transmission electron microscopy (TEM), X-ray powder diffraction (XRD), temperature programmed reduction (TPR), X-ray photoelectron spectroscopy (XPS), and in-situ diffuse reflectance infrared Fourier transform spectroscopy (DRIFTS)). In addition, the influence of catalyst preparation methods (successive impregnation, co-impregnation) has also been studied.

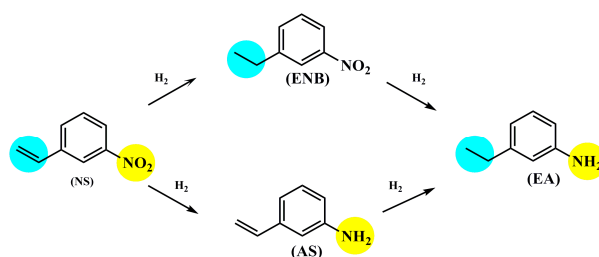
2. Results and Discussion

The preparation of catalysts is described here in brief. Supported Pt catalysts were prepared by wet impregnation using H₂PtCl₆·6H₂O as a metal precursor and P-containing activated charcoal (PAC) and activated carbon (AC) as supports, which were monometallic Pt/PAC and bimetallic Co/Pt/PAC and Co/Pt/AC samples, the latter being prepared by loading Co from Co(NO₃)₂·6H₂O to reduced Pt/PAC and Pt/AC, respectively. In addition, another bimetallic CoPt/PAC sample was prepared by co-impregnation and a monometallic Co/PAC one by impregnation. The final thermal treatment of those samples was reduction with H₂ at 385 °C and 450 °C for Pt-containing and monometallic Co samples, respectively. The catalysts included Pt in a fixed amount of 0.50 wt.-% and Co in different amounts of 0.075, 0.15, and 0.30 wt.-%. The molar ratio of Co/Pt was 1 at a Co loading of 0.15 wt.-%. The detailed catalyst preparation procedures and conditions used are described below in the Experimental Section.

2.1. Catalytic Performance

The performance of those Pt catalysts prepared was tested in liquid phase selective hydrogenation of 3-nitrostyrene (NS) in toluene (Scheme 1), in which 3-aminostyrene (AS), 3-ethylnitrobenzene (ENB), and 3-ethylaniline (EA) would be formed via hydrogenation of nitro group, vinyl one, and both ones, respectively. The product selectivity, as well as the rate of NS conversion, was observed to depend on the catalysts used. Table 1 gives the performance of several monometallic and bimetallic catalysts. Pt on PAC was active and selective to the formation of AS with a selectivity of 81% (entry 2) while Co was inactive (entry 1). The addition of inactive Co to Pt/PAC (Co/Pt = 1) decreased the rate of NS

conversion but increased the AS selectivity to 94% (entry 3 and entry 4). With this catalyst, the nitro group of NS was more selectively hydrogenated to AS than the vinyl group of NS and the vinyl group of AS was little hydrogenated to the final product of EA. However, when AC containing no P species on its surface was used instead of PAC, the modified Co/Pt/AC catalyst had a higher activity but a low selectivity to AS, with which the selectivity to either ENB or EA was larger (entry 5). Even when PAC was used but Pt and Co were loaded simultaneously by co-impregnation, larger NS conversion and smaller AS selectivity were observed (entry 6), similar to Co/Pt/AC, compared to Co/Pt/PAC. That is, the influence of support materials and metal impregnation methods was significant in determining the catalytic activity and the product selectivity.



Scheme 1. Reaction pathways for the hydrogenation of 3-nitrostyrene (NS).

Table 1. Hydrogenation of 3-nitrostyrene (NS) over different catalysts.

Entry	Catalysts	Time (h)	Conversion (%)	Selectivity (%)			
				AS	ENB	EA	Others ^a
1	Co/PAC	6	0	0	0	0	0
2	Pt/PAC	8	94	81	2	15	2
3	Co/Pt/PAC	10	84	94	0	2	4
4	Co/Pt/PAC	14	97	94	1	2	3
5	Co/Pt/AC	1	95	15	24	46	15
6	CoPt/PAC	1	88	12	35	40	13

Reaction conditions: 40 mg catalyst (Pt loading was 0.50 wt.-% and Co loading was 0.15 wt.-%, Co/Pt = 1), 5 mL toluene, 0.5 mmol NS, 100 °C, 4 MPa H₂. ^a Others are traces of 3-hydroxylamine styrene, 3-azostyrene, 3-azoxystyrene, and 3-vinyl nitrosobenzene.

Then, the influence of Co loading was examined using Co/Pt/PAC catalyst that was selective to the formation of AS. The results collected by using Co/Pt values of 0.5, 1.0, and 2.0 are given in Table 2. Although a small added amount of Co (0.075 wt.-%) decreased the rate of NS conversion by a factor of about 2, the selectivity to AS was enhanced to 95% from 81% (entry 2). Further increase in the Co loading did not change the high AS selectivity but increased the catalytic activity (entries 3, 4). The rate of NS conversion with 0.30 wt.-% Co-loaded Pt/PAC was comparable to that with Co-unmodified Pt/PAC (entries 1, 4). The product selectivity with Co/Pt/PAC catalysts was not observed to change with the NS conversion. The time-selectivity-conversion relation measured for a selected catalyst of 0.075 wt.-% Co-loaded Pt/PAC catalyst is given in Figure 1.

Table 2. Hydrogenation of NS over Co-modified 0.50 wt.-% Pt/PAC catalysts.

Entry	Content of Co (wt.-%)	Co/Pt	Time (h)	Conversion (%)	Selectivity (%)				Average Reaction Rate (mmol·g ⁻¹ ·h ⁻¹) ^b
					AS	ENB	EA	Others ^a	
1	0	0	8	94	81	2	15	2	1.5
2	0.075	0.5	16	81	95	0	1	4	0.7
3	0.15	1	10	84	94	0	2	4	1.1
4	0.30	2	8	81	92	0	4	4	1.5

Reaction conditions: 40 mg catalyst (Pt loading was 0.50 wt.-%), 5 mL toluene, 0.5 mmol NS, 100 °C, 4 MPa H₂. ^a Others were 3-hydroxylamine styrene, 3-azostyrene, 3-azoxystyrene, and 3-vinyl nitrosobenzene. ^b Average reaction rate = amount (mole) of NS consumed per 1 g catalyst per 1 h.

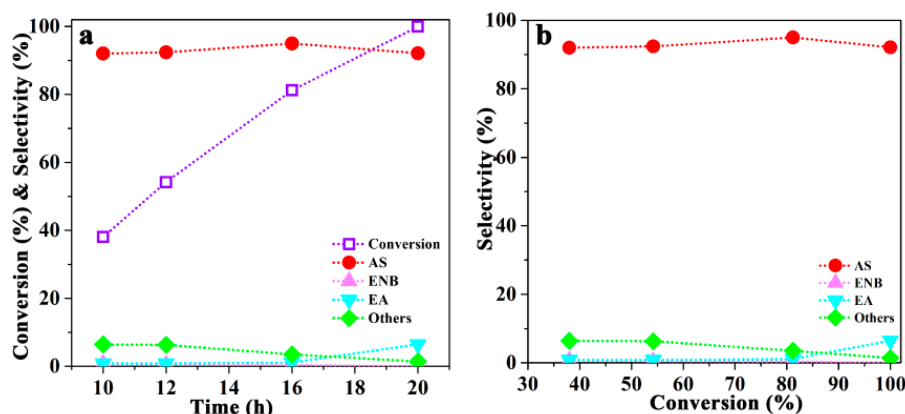


Figure 1. Catalytic performance of 0.075 wt.-% Co-loaded Pt/P-containing activated charcoal (PAC) catalyst in selective hydrogenation of NS. The profile of Time-Conversion-Selectivity (a) and the profile of Conversion-Selectivity (b). (Reaction conditions: 40 mg catalyst, 5 mL toluene, 0.5 mmol NS, 100 °C, 4 MPa H₂).

2.2. Catalyst Characterization

The catalytic performance (activity and selectivity) of supported Pt catalysts was shown to depend significantly on Co addition, support materials (PAC, AC), and metal loading methods (successive impregnation, co-impregnation) as above-mentioned. The high AS selectivity obtained with Co/Pt/PAC catalysts attracted our attention. The catalysts were characterized by different methods to find reasons for such a high AS selectivity in NS hydrogenation, and then the roles of Co additives and P-containing groups on the surface of PAC were discussed.

The dispersion of metal particles on PAC was examined by TEM and XRD. Figure 2 gives TEM images and particle size distributions determined from them for Pt/PAC, Co/Pt/PAC, and CoPt/PAC samples. For the monometallic Pt/PAC catalyst, Pt was finely dispersed in the form of nanoparticles with an average particle size of about 2 nm (Figure 2a). The addition of Co in either 0.15 or 0.30 wt.-% to Pt/PAC (Pt 0.50 wt.-%) increased the size of dispersed metal particles by a factor of about three, which were in the range of 4 to 10 nm (Figure 2b,c). For those Co-modified Pt catalysts, the molar ratio of Co/Pt was 1 or 2. In addition, the size of metal particles in co-impregnated CoPt/PAC was about 2.5 nm (Figure 2d), which was similar to Pt/PAC but different from Co/Pt/PAC samples. XRD results (Figure 3) showed no detectable diffraction of metals and metal oxides probably due to small metal loading and high metal dispersion. The authors believe that Co species were likely to deposit close to or on Pt nanoparticles that already existed on PAC in advance of Co impregnation but not on PAC separately from Pt particles.

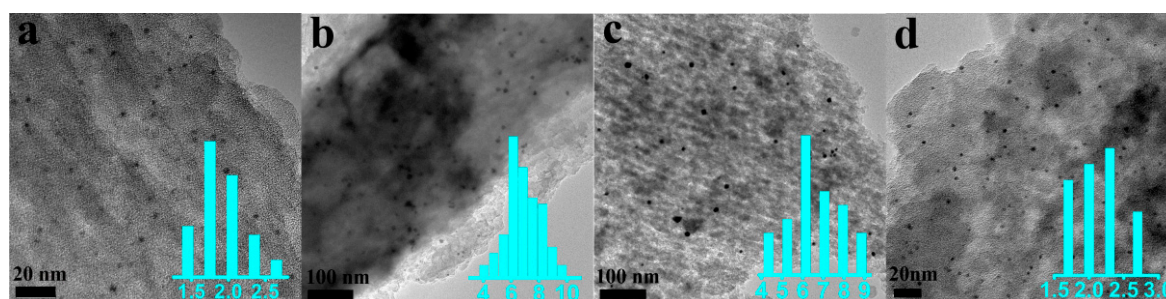


Figure 2. Transmission electron microscopy (TEM) images of 0.50 wt.-% Pt supported PAC catalysts: (a) Pt/PAC, (b) 0.15 wt.-% Co-modified Pt/PAC, (c) 0.30 wt.-% Co-modified Pt/PAC and (d) CoPt/PAC (Prepared by co-impregnated, Co loading was 0.15 wt.-%).

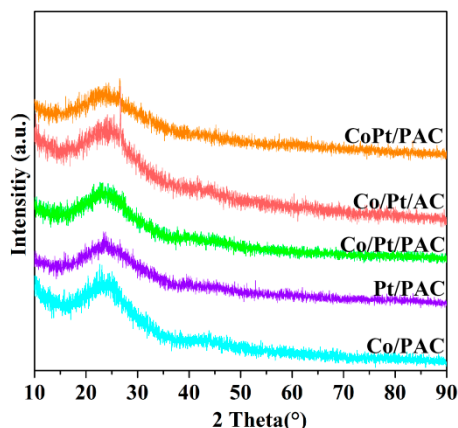


Figure 3. The X-ray powder diffraction (XRD) profiles of different catalysts. (Pt loading was 0.50 wt.-% and Co loading was 0.15 wt.-%).

The behavior of reduction of those samples with H_2 was examined by temperature programmed reduction (TPR), as shown in Figure 4. The metal-unloaded carbon support, PAC, indicated H_2 consumption at 500 to 600 °C, which was used for the removal of surface oxygen-containing functional groups (SOFGs including PO_x , explained later) on PAC. For 0.50 wt.-% Pt-loaded PAC, there were a few different states of Pt species and H_2 consumption was detected at temperatures of 150, 300, 450, and 550 °C, which were assignable to the reduction of free Pt species to Pt^0 , the reduction of those interacting with surface acidic groups, the reduction of Pt- PO_x species, and the removal of SOFGs [51,52]. A broad H_2 consumption was observed at temperatures of 300 to 600 °C for 0.15 wt.-% Co-loaded PAC, due to the reduction of CoO_x and $CoPO_x$ species and SOFGs [43,53,54]. For a bimetallic Co/Pt/PAC catalyst (Co/Pt = 1), in which Pt/PAC was pre-reduced at a low temperature of 150 °C and then loaded with Co, a sharp H_2 consumption peak was observed at 330 °C for the reduction of CoO_x species; in this catalyst, Pt species was almost reduced in advance and so metallic Pt species promoted the reduction of CoO_x species, lowering their reduction temperature to 330 °C from 400 °C [43]. For another CoPt/PAC catalyst prepared by co-impregnation, however, H_2 was consumed in a wide range of temperature, similar to Co/PAC, and Pt had no influence on the reduction of Co species.

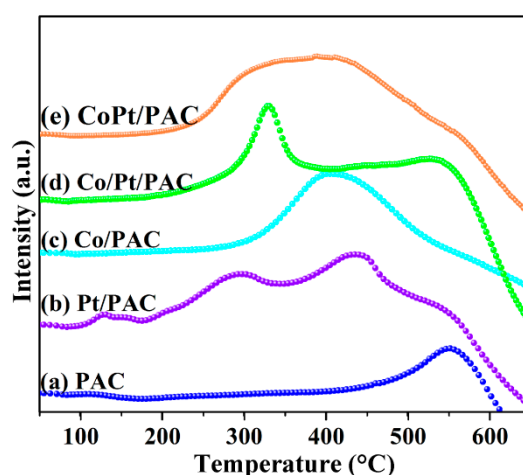


Figure 4. H_2 -temperature programmed reduction (TPR) profiles of PAC (a), monometallic catalysts Pt/PAC (b), Co/PAC (c), bimetallic catalysts Co/Pt/PAC (d), and CoPt/PAC (e). (Pt loading was 0.50 wt.-% and Co loading was 0.15wt.-%, the molar ratio of Co/Pt is 1).

Next, the surface of PAC support and Co-modified and unmodified Pt catalysts on PAC was examined by XPS. Co 2p XPS profiles of monometallic catalysts Co/PC, bimetallic catalysts Co/Pt/PAC

and CoPt/PAC catalysts are shown in Figure 5. The Co 2p_{3/2} peaks of these two samples were close to 784.0 eV, indicating that the surface Co was mainly in the oxidation state of Co^{δ+}, possibly in the form of CoO_x and Co(HPO₃H)₂ [55], which was related to the re-oxidation of the reduced Co in air. In the case of Co/Pt/PAC, the peak at a higher binding energy of 788.7 eV was assigned to Co²⁺ satellite peak in the oxidized state [56]. The binding energy of about 777.3 eV was attributed to CoPO_x species [53,55]. In addition, only a very weak signal at 778.6 eV assigned to Co⁰ was detected on the Co/Pt/PAC catalyst (Co/Pt = 2), but it was absent in the monometallic catalyst Co/PAC. Furthermore, compared with Co/PAC, the signals of Co/Pt/PAC shifted to a higher binding energy area but no binding energy shift for CoPt/PAC. The electronic states of Co indicated that almost all the Co species existed in oxidation states other than metallic states in the monometallic and bimetallic catalysts. Noteworthy, almost no Pt signal can be detected in the XPS of the Co/Pt/PAC and CoPt/PAC catalysts due to the small Pt loading and coverage of Pt with Co species.

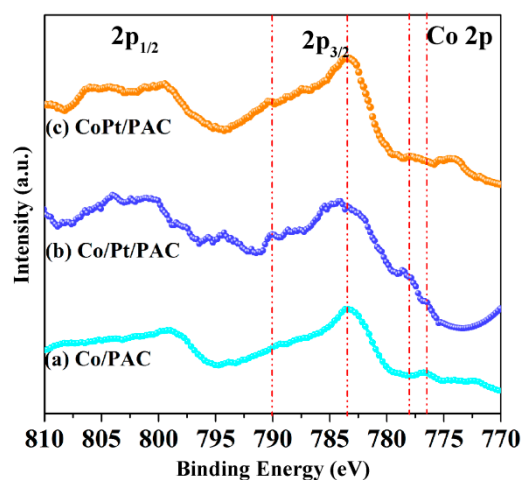


Figure 5. X-ray photoelectron spectroscopy (XPS) profiles of Co 2p of Co/PAC (a), Co/Pt/PAC (b) (Co loading was 0.30 wt.-%) and CoPt/PAC (c) (Co loading was 0.15 wt.-%)(Pt loading was 0.50 wt.-% for all the catalyst).

P in the supports had significant influence on the state of metals loaded on them. P 2p XPS showed the various P species in the monometallic and bimetallic catalysts as seen in Figure 6. The proportions of each P species are also given in Table 3. The deconvolution of the P 2p peaks was used to evaluate the four contributions at 130.6 eV (P-1), 133.3 eV (P-2), 134.5 eV (P-3), and 135.9 eV (P-4), which were related to the phosphine, phosphinic, phosphite, and phosphate, respectively [57,58]. The more coordinated oxygen atoms the P species coordinated, the higher the binding energy was. P-1 existed in all the monometallic and bimetallic catalysts although the amount is significantly less. The content of P-2 species in the Co/Pt/PAC catalysts was larger than that in Pt/PAC, Co/PAC, and CoPt/PAC, and it was also influenced by the Co/Pt ratio in the catalysts (Table 3). The addition of Co increased the content of low-coordinated P species of phosphinic (P-2 species) in Co/Pt/PAC catalysts but not in CoPt/PAC. Furthermore, P-4 species in Co/PAC and CoPt/PAC catalysts showed the largest percentage of 31.9% and 27.4%, compared to Pt/PAC (5.3%) and Co/Pt/PAC (<4%). It is proposed that the CoO_x and CoPO_x in the Co/Pt/PAC were dispersed uniformly on the Pt, which caused the transformation of P-4 to P-2 during the reduction. The influence of P species on the hydrogenation selectivity to -NO₂ group of NS will be discussed in detail in the following section.

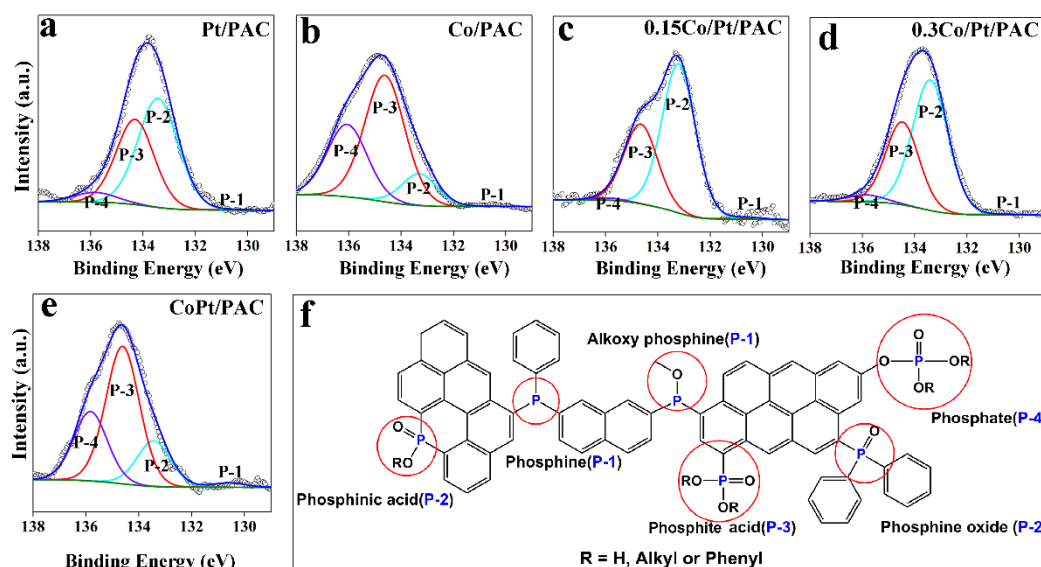


Figure 6. P 2p XPS spectra of Pt/PAC (a), Co/PAC (b), 0.15 wt.-% Co-modified Pt/PAC (c), 0.30 wt.-% Co-modified Pt/PAC (d), CoPt/PAC (e) (Co loading was 0.15 wt.-%), and (f) Types of P-containing functional groups in the activated charcoal.

Table 3. The content of different P-containing functional groups over bimetallic and monometallic catalysts.

Entry	Catalysts ^a	Co/Pt Molar Ratio	Content of P-containing Functional Groups (%)			
			Phosphine (P-1)	Phosphonic (P-2)	Phosphite (P-3)	Phosphate (P-4)
1	Pt/PAC	0	0.3	54.4	40.1	5.2
2	0.15Co/PAC	∞	0.1	12.4	55.6	31.9
3	0.15Co/Pt/PAC	1	0.5	64.3	34.3	0.9
4	0.30Co/Pt/PAC	2	0.7	60.2	35.8	3.3
5	0.15CoPt/PAC	1	0.2	18.0	54.4	27.4

^a Pt loading was 0.50 wt.-% for all catalysts; Co loading was given before Co in wt.-%.

Furthermore, the adsorption of NS substrate was examined by in-situ DRIFTS for Co/Pt/PAC and CoPt/PAC that were selective to AS and to ENB and EA, respectively. These samples contained Pt and Co in 0.50 and 0.15 wt.-%, respectively (Co/Pt = 1) and were both reduced by H₂ at 385 °C. Figure 7 gives in-situ DRIFTS spectra recorded at 150 °C just after the NS adsorption and after the removal of physically adsorbed NS molecules by passing a He gas stream for 2 h. Two absorption bands were observed at 1350 and 1530 cm⁻¹ assignable to $\nu_{as}(\text{NO}_2)$ and $\nu_s(\text{NO}_2)$ of the nitro group of NS [59–62] and three overlapped bands at 2870 to 3000 cm⁻¹ due to –CH of =C–H on the benzene ring [63,64]. These absorption bands remained unchanged after passing He gas over the sample, through which, however, the absorption band at 3090 cm⁻¹ disappeared due to (–CH) of the vinyl group stretching vibration [65]. That is, the substrate NS was adsorbed with its nitro group on the catalyst group more strongly than with its vinyl group. For CoPt/PAC catalyst, in contrast, those absorption bands were detected even after the sample was purged by He due to the nitro and vinyl groups of NS. Therefore, NS was adsorbed with the nitro and vinyl groups on CoPt/PAC while preferentially with the nitro group on Co/Pt/PAC. This difference in the NS adsorption behavior is an important factor responsible for the differences observed in the product selectivity in the NS hydrogenation between the two catalysts.

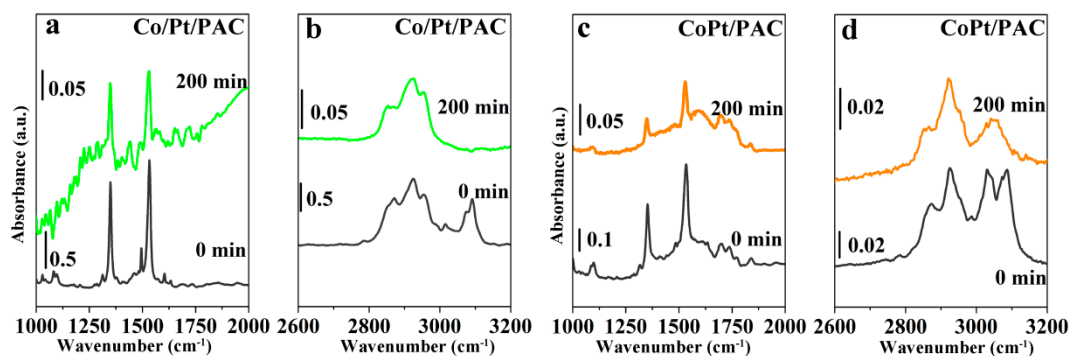


Figure 7. In-situ diffuse reflectance infrared Fourier transform spectroscopy (DRIFTS) adsorption spectra of NS over Co/Pt/PAC (a,b) and CoPt/PAC (c,d). (Pt loading was 0.50 wt.-% and Co loading is 0.15 wt.-%).

3. Roles of Co Additive and Surface P-containing Species

The present results demonstrate that the high selectivity to AS in NS hydrogenation can be achieved by Co/Pt/PAC catalyst but not by Pt/PAC, CoPt/PAC, and Co/Pt/AC ones. That is, both Co additive and P-containing carbon are requisites, and Co is required to be loaded by successive impregnation to pre-reduced Pt/PAC. The high AS selectivity results from the preferential adsorption of NS with its nitro group on the catalyst, indicating that the surface structure of supported bimetallic metal particles should be beneficial for such selective adsorption. According to the present TEM and XPS results and those reported in previous work on Pt/PAC, a possible structure of the supported Pt particles that interact with and are modified by Co and P species is proposed, as in Figure 8. The authors have previously shown that the selectivity of NS hydrogenation over carbon-supported Pt catalyst is switched, becoming selective to AS, by the decoration of Pt particles with PO_x species. The surface of Pt particles is covered in part by PO_x species and the resulting Pt–PO_x interface favors the adsorption of NS with its polar nitro group rather than the non-polar vinyl group. This results in the selective hydrogenation of the nitro group of NS yielding AS, the vinyl group of which is not adsorbed and hydrogenated to the final product of EA. The partial decoration with PO_x decreases the number of active Pt sites exposed on the surface of Pt particles, decreasing the overall rate of NS hydrogenation. In a monometallic Pt/PAC catalyst using a P-containing support, some Pt species interact with PO_x ones at the Pt particle–support interface and this interfacial layer assists the adsorption of NS with its nitro group rather than vinyl group (Figure 8). In addition, such Pt–PO_x interactions should affect the surface electronic properties of Pt particles. Then, the adsorption and hydrogenation of nitro group of NS are likely to occur selectively on this Pt/PAC catalyst, as reported previously [50]. For the Pt–PO_x interactions, P-2 type of surface P species is important (Table 3). When Co is added to pre-reduced Pt/PAC catalyst, it tends to deposit close to and/or on the Pt particles and to increase the amount of P-2 type P species. Then, the addition of Co should increase the number of Pt species interacting with the PO_x ones at the Pt particle–support interface and cover the surface of Pt particles to some extent. The electronic properties of surface Pt species would also be influenced by the presence of more PO_x species at the interface and some CoO_x species on the Pt particles. These factors should be responsible for a larger AS selectivity via hydrogenation of nitro group of NS observed in the Co-modified Pt/PAC catalyst. For CoPt/PAC catalyst prepared by co-impregnation, such a modification of Pt particles by PO_x and/or CoO_x is even less significant. It is likely that CoO_x species interact with PO_x (P-3) more strongly than that of Pt with PO_x (P-2), resulting in less or no significant modification of the surface of Pt particles by these species. Then, the CoPt/PAC catalyst is not selective to the formation of AS (Table 1).

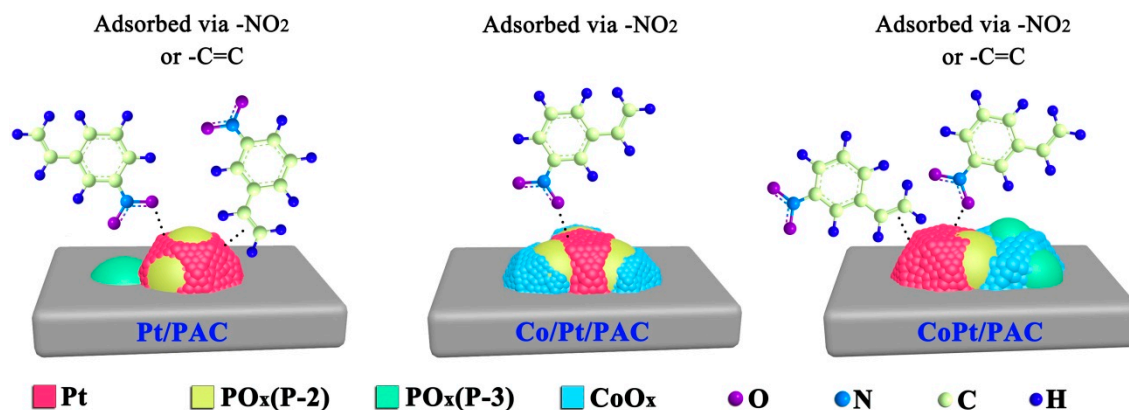


Figure 8. Possible structures of Pt/PAC, Co/Pt/PAC and CoPt/PAC catalysts and different modes of adsorption of NS on their metal particles. (Red: Pt, Yellow: PO_x (P-2), Green: PO_x (P-3), Blue: CoO_x).

4. Experimental Section

4.1. Materials

Commercially available reagents, 3-nitrostyrene (Acros; $\geq 97\%$), $\text{H}_2\text{PtCl}_6 \cdot 6\text{H}_2\text{O}$ (Shanghai Jiu Ling, Shanghai, China; $\geq 99.9\%$), $\text{Co}(\text{NO}_3)_2 \cdot 6\text{H}_2\text{O}$ (Aladin, Shanghai, China; $\geq 99.9\%$), toluene and ethanol (Beijing chemicals, Beijing, China; $\geq 99.9\%$) were used as received. The P-containing activated charcoal (Sigma-Aldrich, St. Louis, MO, USA, untreated powder, 100–400 mesh, C3345, 1.7 wt.-% phosphor in weight percentage, surface area is $1262 \text{ m}^2/\text{g}$) and activated coconut carbon without P elements (Fujian XinSen, Nanping, China, C $\geq 99.0\%$, ash $\leq 0.50\%$, bulk density $0.32\text{--}0.4 \text{ kg/L}$, surface area is $1851 \text{ m}^2/\text{g}$) were used as raw carbon materials, which are abbreviated as PAC and AC.

4.2. Catalyst Preparation

Supported monometallic (Pt/PAC, Co/PAC) and bimetallic (Co/Pt/PAC, Co/Pt/AC, CoPt/PAC) catalysts were prepared by the wet-impregnation method. In the synthesis of 0.50 wt.-% Pt/PC catalyst, 13.3 mg $\text{H}_2\text{PtCl}_6 \cdot 6\text{H}_2\text{O}$ was dissolved in 10 mL ethanol, and then 1.0 g carbon support was added to form a slurry mixture. The slurry was dried at $80 \text{ }^\circ\text{C}$ in a water bath with stirring and then kept at $80 \text{ }^\circ\text{C}$ in an oven overnight. Finally, the sample was reduced in an H_2 stream at $385 \text{ }^\circ\text{C}$ for 2 h. Similarly, Co was impregnated to PAC from $\text{Co}(\text{NO}_3)_2$, calcined in N_2 at $300 \text{ }^\circ\text{C}$ for 2 h, and then reduced in H_2 at $450 \text{ }^\circ\text{C}$ for 2 h. For bimetallic Co/Pt/PAC and Co/Pt/AC, a given amount of Co precursor ethanol solution was added drop by drop to a monometallic Pt sample that was pre-reduced at $150 \text{ }^\circ\text{C}$ for 2 h and the sample obtained was dried at $80 \text{ }^\circ\text{C}$, calcined in N_2 at $300 \text{ }^\circ\text{C}$, and then reduced in H_2 at $385 \text{ }^\circ\text{C}$ for 2 h. Another bimetallic CoPt/PAC was prepared by co-impregnation using the same metal precursors in ethanol. After co-impregnation, the bimetallic sample was calcined in N_2 at $300 \text{ }^\circ\text{C}$ and then reduced in H_2 at $385 \text{ }^\circ\text{C}$ for 2 h. After the above-mentioned reduction and cooling to ambient temperature, all the Pt containing catalysts were purged with N_2 for 30 min and then stored in air before use, and the Co/PAC catalyst was used directly after purging with N_2 .

4.3. Characterization

The monometallic and bimetallic catalysts so prepared were characterized by the following methods. Transmission electron microscopy (TEM) images were collected on a JEOL (Tokyo, Japan) JEM-2010 instrument operated at an accelerating voltage of 200 kV. X-ray photoelectron spectroscopy (XPS) measurements were carried on VG Microtech (Eugene, OR, USA) 3000 Multilab without sputtering. X-ray powder diffraction (XRD) measurements were carried on a Bruker (Bremen, Germany) D8 ADVANCE diffractometer, using $\text{Cu K}\alpha$ radiation ($\lambda = 0.154 \text{ nm}$). Temperature programmed reduction (TPR) using H_2 was measured on Micromeritics AutoChem (Norcross, GA, USA) II 2920. For H_2 -TPR, a sample (50 mg) was treated with an Ar stream (50 mL/min) at $100 \text{ }^\circ\text{C}$ for 1 h to remove H_2O and

cooled to 50 °C. Then, the sample was heated at 5 °C/min to 700 °C in a stream of 10% H₂ in Ar at a flow rate of 50 mL/min. The amount of H₂ consumed was measured by a gas chromatograph with a thermal conductivity detector. The adsorption of 3-nitrostyrene was examined by in situ diffuse reflectance infrared Fourier transform spectroscopy (DRIFTS) on Thermo Scientific Nicolet (Waltham, MA, USA) 6700 Fourier transform infrared spectroscopy. A catalyst sample was reduced in an FTIR cell with 10% H₂/Ar mixture (30 mL/min) at 385 °C for 30 min and then cooled to 30 °C. The cell was purged with a He stream (30 mL/min) for 30 min, and the background spectrum was recorded. After the addition of 40 µL substrate (0.5 M in toluene) to the sample, the cell was heated to 150 °C slowly while passing heat 30 mL/min. The spectrum was recorded at 150 °C every 30 min until all the physically adsorbed species were removed.

4.4. Hydrogenation

The catalytic performances of monometallic and bimetallic catalysts were tested for the selective hydrogenation of NS using a 50 mL stainless steel autoclave with an inner Teflon coating. For a typical catalytic reaction, 0.5 mmol NS and 40 mg catalyst were mixed in 5 mL toluene. The reactor was sealed and purged with 1 MPa H₂ three times. And then 4 MPa H₂ introduced to the reactor after preheating at 100 °C for 20 min. The products were analyzed by gas chromatography (Shimadzu, Kyoto, Japan, 2010) equipped with a capillary column (Restek (Bellefonte, PA, USA) Rtx-5 30 m × 0.25 mm × 0.25 µm) and a flame ionization detector (FID).

5. Conclusions

The product selectivity in liquid phase NS hydrogenation over supported Pt catalyst can be controlled by using P-containing carbon support (PAC) and Co additive, which enhance the selectivity to the hydrogenation of its nitro group compared to the vinyl group, yielding AS in a high selectivity. There is an interfacial layer of Pt-PO_x on the surface of supported Pt particles and this layer is beneficial for the preferential adsorption of the substrate molecule with its polar nitro group and its subsequent hydrogenation to AS. The addition of Co species influences the nature of surface P species on PAC and assists the formation of Pt-PO_x interfacial area on the surface of Pt particles. The modification of the surface of Pt particles with PO_x species decreases the number of active Pt⁰ sites, and so causes a reduction in the rate of NS hydrogenation. The promotional effect of surface P and Co additive species on the AS selectivity appears for Co/Pt/PAC catalyst prepared by successive impregnation of Pt and then Co. No promotional effect is unlikely for CoPt/PAC prepared by co-impregnation, which does not produce a surface on Pt particles favoring the preferential adsorption of NS with its nitro group. The product selectivity with CoPt/PAC is similar to that with monometallic Pt catalyst on P-free AC support.

Author Contributions: Conceptualization, Q.W. and C.Z.; Data curation, Q.W.; Formal analysis, Q.W. and C.Z.; Funding acquisition, C.Z. and F.Z.; Project administration, F.Z.; Supervision, C.Z. and F.Z.; Validation, Q.W., W.L. and H.C.; Writing—original draft, Q.W.; Writing—review and editing, C.Z., M.A. and F.Z.

Funding: This research was funded by National Program on Key Research Project, 2016YFA0602900; National Natural Science Foundation of China, 21872134, 21473179; International Cooperation Project of Jilin Province, 20170414012GH; the Youth Innovation Promotion Association, 2014203; Chinese Academy of Science, and CAS President's International Fellowship Initiative (PIFI) 2018CV0012, Chinese Academy of Science.

Conflicts of Interest: The authors declare no conflict of interest.

References

1. Cao, Y.; Mao, S.; Li, M.; Chen, Y.; Wang, Y. Metal/porous carbon composites for heterogeneous catalysis: Old catalysts with improved performance promoted by N-doping. *ACS Catal.* **2017**, *7*, 8090–8112. [[CrossRef](#)]
2. Lin, R.; Albani, D.; Fako, E.; Kaiser, S.K.; Safonova, O.V.; López, N.; Pérez-Ramírez, J. Design of single gold atoms on nitrogen-doped carbon for molecular recognition in alkyne semi-hydrogenation. *Angew. Chem. Int. Ed.* **2019**, *58*, 504–509. [[CrossRef](#)] [[PubMed](#)]

3. Li, J.; Tu, D.; Li, Y.; Wang, W.; Yu, Q.; Yang, J.; Lu, J. Co-N-doped carbon nanotubes supported on diatomite for highly efficient catalysis oxidative carbonylation of amines with CO and air. *Appl. Catal. A Gen.* **2018**, *549*, 112–116. [[CrossRef](#)]
4. Hu, X.; Long, Y.; Fan, M.; Yuan, M.; Zhao, H.; Ma, J.; Dong, Z. Two-dimensional covalent organic frameworks as self-template derived nitrogen-doped carbon nanosheets for eco-friendly metal-free catalysis. *Appl. Catal. B Environ.* **2019**, *244*, 25–35. [[CrossRef](#)]
5. Ruiz-García, C.; Heras, F.; Calvo, L.; Alonso-Morales, N.; Rodriguez, J.J.; Gilarranz, M.A. Platinum and N-doped carbon nanostructures as catalysts in hydrodechlorination reactions. *Appl. Catal. B Environ.* **2018**, *238*, 609–617. [[CrossRef](#)]
6. Gao, Y.; Zhao, H.; Chen, D.; Chen, C.; Ciucci, F. In situ synthesis of mesoporous manganese oxide/sulfur-doped graphitized carbon as a bifunctional catalyst for oxygen evolution/reduction reactions. *Carbon* **2015**, *94*, 1028–1036. [[CrossRef](#)]
7. Yang, S.; Peng, L.; Oveisi, E.; Bulut, S.; Sun, D.T.; Asgari, M.; Trukhina, O.; Queen, W.L. MOF-derived cobalt phosphide/carbon nanocubes for selective hydrogenation of nitroarenes to anilines. *Chem. Eur. J.* **2018**, *24*, 4234–4238. [[CrossRef](#)] [[PubMed](#)]
8. Berenguer, A.; Sankaranarayanan, T.M.; Gómez, G.; Moreno, I.; Coronado, J.M.; Pizarro, P.; Serrano, D.P. Evaluation of transition metal phosphides supported on ordered mesoporous materials as catalysts for phenol hydrodeoxygenation. *Green Chem.* **2016**, *18*, 1938–1951. [[CrossRef](#)]
9. Sweeny, N.P.; Rohrer, C.S.; Brown, O.W. Dinickel phosphide as a heterogeneous catalyst for the vapor phase reduction of nitrobenzene with hydrogen to aniline and water. *J. Am. Chem. Soc.* **1958**, *80*, 799–800. [[CrossRef](#)]
10. Zhang, P.; Gong, Y.; Li, H.; Chen, Z.; Wang, Y. Solvent-free aerobic oxidation of hydrocarbons and alcohols with Pd@N-doped carbon from glucose. *Nat. Commun.* **2013**, *4*, 1593. [[CrossRef](#)]
11. Chao, S.; Zou, F.; Wan, F.; Dong, X.; Wang, Y.; Wang, Y.; Guan, Q.; Wang, G.; Li, W. Nitrogen-doped carbon derived from ZIF-8 as a high-performance metal-free catalyst for acetylene hydrochlorination. *Sci. Rep.* **2017**, *7*, 39789. [[CrossRef](#)]
12. Duan, X.; O'Donnell, K.; Sun, H.; Wang, Y.; Wang, S. Sulfur and nitrogen Co-doped graphene for metal-free catalytic oxidation reactions. *Small* **2015**, *11*, 3036–3044. [[CrossRef](#)] [[PubMed](#)]
13. Shi, W.; Zhang, B.; Lin, Y.; Wang, Q.; Zhang, Q.; Su, D.S. Enhanced chemoselective hydrogenation through tuning the interaction between Pt nanoparticles and carbon supports: Insights from identical location transmission electron microscopy and X-ray photoelectron spectroscopy. *ACS Catal.* **2016**, *7*, 7844–7854. [[CrossRef](#)]
14. Zhang, X.; Wang, N.; Geng, L.; Fu, J.; Hu, H.; Zhang, D.; Zhu, B.; Carozza, J.; Han, H. Facile synthesis of ultrafine cobalt oxides embedded into N-doped carbon with superior activity in hydrogenation of 4-nitrophenol. *J. Colloid Interface Sci.* **2018**, *512*, 844–852. [[CrossRef](#)] [[PubMed](#)]
15. Zhu, Y.; Yu, G.; Yang, J.; Yuan, M.; Xu, D.; Dong, Z. Biowaste soybean curd residue-derived Pd/nitrogen-doped porous carbon with excellent catalytic performance for phenol hydrogenation. *J. Colloid Interface Sci.* **2019**, *533*, 259–267. [[CrossRef](#)] [[PubMed](#)]
16. Fiorio, J.L.; Gonçalves, R.V.; Teixeira-Neto, E.; López, N.; Rossi, L.M. Accessing frustrated lewis pair chemistry through robust gold@N-doped carbon for selective hydrogenation of alkynes. *ACS Catal.* **2018**, *8*, 3516–3524. [[CrossRef](#)]
17. Pisduangdaw, S.; Mekasuwandumrong, O.; Fujita, S.I.; Arai, M.; Yoshida, H.; Panpranot, J. One step synthesis of Pt–Co/TiO₂ catalysts by flame spray pyrolysis for the hydrogenation of 3-nitrostyrene. *Catal. Commun.* **2015**, *61*, 11–15. [[CrossRef](#)]
18. Chu, K.; Wang, F.; Tian, Y.; Wei, Z. Phosphorus doped and defects engineered graphene for improved electrochemical sensing: Synergistic effect of dopants and defects. *Electrochim. Acta* **2017**, *231*, 557–564. [[CrossRef](#)]
19. Ayusheev, A.B.; Taran, O.P.; Seryak, I.A.; Podyacheva, O.Y.; Descorme, C.; Besson, M.; Kibis, L.S.; Boronin, A.I.; Romanenko, A.I.; Ismagilov, Z.R.; et al. Ruthenium nanoparticles supported on nitrogen-doped carbon nanofibers for the catalytic wet air oxidation of phenol. *Appl. Catal. B Environ.* **2014**, *146*, 177–185. [[CrossRef](#)]
20. Zhao, L. Natural phosphorus-doped honeycomb carbon materials as oxygen reduction catalysts derived from pulsatilla chinensis (bunge) regel. *RSC Adv.* **2017**, *7*, 13904–13910. [[CrossRef](#)]

21. Lu, C.; Wang, M.; Feng, Z.; Qi, Y.; Feng, F.; Ma, L.; Zhang, Q.; Li, X. A phosphorus–carbon framework over activated carbon supported palladium nanoparticles for the chemoselective hydrogenation of para-chloronitrobenzene. *Catal. Sci. Technol.* **2017**, *7*, 1581–1589. [[CrossRef](#)]
22. Hita, I.; Cordero-Lanzac, T.; Gallardo, A.; Arandes, J.M.; Rodríguez-Mirasol, J.; Bilbao, J.; Cordero, T.; Castaño, P. Phosphorus-containing activated carbon as acid support in a bifunctional Pt–Pd catalyst for tire oil hydrocracking. *Catal. Commun.* **2016**, *78*, 48–51. [[CrossRef](#)]
23. Liu, Z.; Shi, Q.; Zhang, R.; Wang, Q.; Kang, G.; Peng, F. Phosphorus-doped carbon nanotubes supported low Pt loading catalyst for the oxygen reduction reaction in acidic fuel cells. *J. Power Sources* **2014**, *268*, 171–175. [[CrossRef](#)]
24. Wang, B.; Yu, L.; Zhang, J.; Pu, Y.; Zhang, H.; Li, W. Phosphorus-doped carbon supports enhance gold-based catalysts for acetylene hydrochlorination. *RSC Adv.* **2014**, *4*, 15877. [[CrossRef](#)]
25. Zhuang, M.; Ou, X.; Dou, Y.; Zhang, L.; Zhang, Q.; Wu, R.; Ding, Y.; Shao, M.; Luo, Z. Polymer-embedded fabrication of Co₂P nanoparticles encapsulated in N,P-doped graphene for hydrogen generation. *Nano Lett.* **2016**, *16*, 4691–4698. [[CrossRef](#)]
26. Song, P.; Zhu, L.; Bo, X.; Wang, A.; Wang, G.; Guo, L. Pt nanoparticles incorporated into phosphorus-doped ordered mesoporous carbons: Enhanced catalytic activity for methanol electrooxidation. *Electrochim. Acta* **2014**, *127*, 307–314. [[CrossRef](#)]
27. Xue, X.; Ge, J.; Liu, C.; Xing, W.; Lu, T. Novel chemical synthesis of Pt–Ru–P electrocatalysts by hypophosphite deposition for enhanced methanol oxidation and CO tolerance in direct methanol fuel cell. *Electrochem. Commun.* **2006**, *8*, 1280–1286. [[CrossRef](#)]
28. Xue, X.; Ge, J.; Tian, T.; Liu, C.; Xing, W.; Lu, T. Enhancement of the electrooxidation of ethanol on Pt–Sn–P/C catalysts prepared by chemical deposition process. *J. Power Sources* **2007**, *172*, 560–569. [[CrossRef](#)]
29. Tong, Y.C.; Zhang, X.Y.; Wang, Q.Y.; Xu, X.J. The adsorption mechanism of platinum on phosphorus-doped single walled carbon nanotube. *Comput. Theor. Chem.* **2015**, *1059*, 1–6. [[CrossRef](#)]
30. Paradies, J. Metal-free hydrogenation of unsaturated hydrocarbons employing molecular hydrogen. *Angew. Chem. Int. Ed.* **2014**, *53*, 3552–3557. [[CrossRef](#)]
31. Wang, L.; Wang, L.; Zhang, J.; Liu, X.; Wang, H.; Zhang, W.; Yang, Q.; Ma, J.; Dong, X.; Yoo, S.J.; et al. Selective hydrogenation of CO₂ to ethanol over cobalt catalysts. *Angew. Chem. Int. Ed.* **2018**, *57*, 6104–6108. [[CrossRef](#)]
32. Wang, C.; Wang, L.; Zhang, J.; Wang, H.; Lewis, J.P.; Xiao, F. Product selectivity controlled by zeolite crystals in biomass hydrogenation over a palladium catalyst. *J. Am. Chem. Soc.* **2016**, *138*, 7880–7883. [[CrossRef](#)]
33. Albani, D.; Shahrokhi, M.; Chen, Z.; Mitchell, S.; Hauert, R.; López, N.; Pérez-Ramírez, J. Selective ensembles in supported palladium sulfide nanoparticles for alkyne semi-hydrogenation. *Nat. Commun.* **2018**, *9*, 2634. [[CrossRef](#)] [[PubMed](#)]
34. Durndell, L.J.; Parlett, C.M.A.; Hondow, N.S.; Isaacs, M.A.; Wilson, K.; Lee, A.F. Selectivity control in Pt-catalyzed cinnamaldehyde hydrogenation. *Sci. Rep.* **2015**, *5*, 9425. [[CrossRef](#)]
35. Hidalgo-Carrillo, J.; Sebti, J.; Marinas, A.; Marinas, J.M.; Sebti, S.; Urbano, F.J. XPS evidence for structure–performance relationship in selective hydrogenation of crotonaldehyde to crotyl alcohol on platinum systems supported on natural phosphates. *J. Colloid Interface Sci.* **2012**, *382*, 67–73. [[CrossRef](#)] [[PubMed](#)]
36. Bornschein, C.; Werkmeister, S.; Wendt, B.; Jiao, H.; Alberico, E.; Baumann, W.; Junge, H.; Junge, K.; Beller, M. Mild and selective hydrogenation of aromatic and aliphatic (di)nitriles with a well-defined iron pincer complex. *Nat. Commun.* **2014**, *5*, 4111. [[CrossRef](#)]
37. Lu, X.; He, J.; Jing, R.; Tao, P.; Nie, R.; Zhou, D.; Xia, Q. Microwave-activated Ni/carbon catalysts for highly selective hydrogenation of nitrobenzene to cyclohexylamine. *Sci. Rep.* **2017**, *7*, 2676. [[CrossRef](#)]
38. Chatterjee, M.; Chatterjee, A.; Kawanami, H.; Ishizaka, T.; Suzuki, T.; Suzuki, A. Rapid hydrogenation of aromatic nitro compounds in supercritical carbon dioxide: Mechanistic implications via experimental and theoretical investigations. *Adv. Synth. Catal.* **2012**, *354*, 2009–2018. [[CrossRef](#)]
39. Wang, K.; Gao, W.; Jiang, P.; Lan, K.; Yang, M.; Huang, X.; Ma, L.; Niu, F.; Li, R. Bi-functional catalyst of porous N-doped carbon with bimetallic FeCu for solvent-free resultant imines and hydrogenation of nitroarenes. *Mole. Catal.* **2019**, *465*, 43–53. [[CrossRef](#)]
40. Budi, C.S.; Saikia, D.; Chen, C.-S.; Kao, H.-M. Catalytic evaluation of tunable Ni nanoparticles embedded in organic functionalized 2D and 3D ordered mesoporous silicas from the hydrogenation of nitroarenes. *J. Catal.* **2019**, *370*, 274–288. [[CrossRef](#)]

41. Sreedhar, B.; Devi, D.K.; Yada, D. Selective hydrogenation of nitroarenes using gum acacia supported Pt colloid an effective reusable catalyst in aqueous medium. *Catal. Commun.* **2011**, *12*, 1009–1014. [[CrossRef](#)]
42. Veerakumar, P.; Thanasekaran, P.; Lin, K.-C.; Liu, S.-B. Well-dispersed rhenium nanoparticles on three-dimensional carbon nanostructures: Efficient catalysts for the reduction of aromatic nitro compounds. *J. Colloid Interface Sci.* **2017**, *506*, 271–282. [[CrossRef](#)] [[PubMed](#)]
43. Wang, X.; He, Y.; Liu, Y.; Park, J.; Liang, X. Atomic layer deposited Pt-Co bimetallic catalysts for selective hydrogenation of α , β -unsaturated aldehydes to unsaturated alcohols. *J. Catal.* **2018**, *366*, 61–69. [[CrossRef](#)]
44. Han, X.; Zhou, R.; Yue, B.; Zheng, X. Selective hydrogenation of cinnamaldehyde over Pt/ZrO₂ catalyst modified by Cr, Mn, Fe, Co and Ni. *Catal. Lett.* **2006**, *109*, 157–161. [[CrossRef](#)]
45. Li, Y.; Zhu, P.-F.; Zhou, R.-X. Selective hydrogenation of cinnamaldehyde to cinnamyl alcohol with carbon nanotubes supported Pt-Co catalysts. *Appl. Surf. Sci.* **2008**, *254*, 2609–2614. [[CrossRef](#)]
46. Tian, Z.; Li, Q.; Hou, J.; Pei, L.; Li, Y.; Ai, S. Platinum nanocrystals supported on CoAl mixed metal oxide nanosheets derived from layered double hydroxides as catalysts for selective hydrogenation of cinnamaldehyde. *J. Catal.* **2015**, *331*, 193–202. [[CrossRef](#)]
47. Tian, Z.; Liu, C.; Li, Q.; Hou, J.; Li, Y.; Ai, S. Nitrogen- and oxygen-functionalized carbon nanotubes supported Pt-based catalyst for the selective hydrogenation of cinnamaldehyde. *Appl. Catal. A Gen.* **2015**, *506*, 134–142. [[CrossRef](#)]
48. Chen, T.; Rodionov, V.O. Controllable catalysis with nanoparticles: Bimetallic alloy systems and surface adsorbates. *ACS Catal.* **2016**, *6*, 4025–4033. [[CrossRef](#)]
49. Wang, H.; Bai, S.; Pi, Y.; Shao, Q.; Tan, Y.; Huang, X. A strongly coupled ultrasmall Pt₃Co nanoparticle-ultrathin Co(OH)₂ nanosheet architecture enhances selective hydrogenation of α , β -unsaturated aldehydes. *ACS Catal.* **2019**, *9*, 154–159. [[CrossRef](#)]
50. Wu, Q.; Zhang, B.; Zhang, C.; Meng, X.; Su, X.; Jiang, S.; Shi, R.; Li, Y.; Lin, W.; Arai, M.; et al. Significance of surface oxygen-containing groups and heteroatom P species in switching the selectivity of Pt/C catalyst in hydrogenation of 3-nitrostyrene. *J. Catal.* **2018**, *364*, 297–307. [[CrossRef](#)]
51. Lu, X.H.; Shen, Y.; He, J.; Jing, R.; Tao, P.P.; Hu, A.; Nie, R.F.; Zhou, D.; Xia, Q.H. Selective hydrogenation of benzoic acid to cyclohexane carboxylic acid over microwave-activated Ni/carbon catalysts. *Mol. Catal.* **2018**, *444*, 53–61. [[CrossRef](#)]
52. Musci, J.J.; Merlo, A.B.; Casella, M.L. Aqueous phase hydrogenation of furfural using carbon-supported Ru and RuSn catalysts. *Catal. Today* **2017**, *296*, 43–50. [[CrossRef](#)]
53. Chang, J.; Xiao, Y.; Xiao, M.; Ge, J.; Liu, C.; Xing, W. Surface oxidized cobalt-phosphide nanorods as an advanced oxygen evolution catalyst in alkaline solution. *ACS Catal.* **2015**, *5*, 6874–6878. [[CrossRef](#)]
54. Prins, R.; Bussell, M.E. Metal phosphides: Preparation, characterization and catalytic reactivity. *Catal. Lett.* **2012**, *142*, 1413–1436. [[CrossRef](#)]
55. Infantes-Molina, A.; Cecilia, J.A.; Pawelec, B.; Fierro, J.L.G.; Rodríguez-Castellón, E.; Jiménez-López, A. Ni₂P and CoP catalysts prepared from phosphite-type precursors for HDS–HDN competitive reactions. *Appl. Catal. A Gen.* **2010**, *390*, 253–263. [[CrossRef](#)]
56. Sennu, P.; Kim, H.S.; An, J.Y.; Aravindan, V.; Lee, Y.S. Synthesis of 2D/2D structured mesoporous Co₃O₄ nanosheet/N-doped reduced graphene oxide composites as a highly stable negative electrode for lithium battery applications. *Chem. Asian J.* **2015**, *10*, 1776–1783. [[CrossRef](#)]
57. Hasegawa, G.; Deguchi, T.; Kanamori, K.; Kobayashi, Y.; Kageyama, H.; Abe, T.; Nakanishi, K. High-level doping of nitrogen, phosphorus, and sulfur into activated carbon monoliths and their electrochemical capacitances. *Chem. Mater.* **2015**, *27*, 4703–4712. [[CrossRef](#)]
58. Patel, M.A.; Luo, F.; Khoshi, M.R.; Rabie, E.; Zhang, Q.; Flach, C.R.; Mendelsohn, R.; Garfunkel, E.; Szostak, M.; He, H. P-doped porous carbon as metal free catalysts for selective aerobic oxidation with an unexpected mechanism. *ACS Nano* **2016**, *10*, 2305–2315. [[CrossRef](#)]
59. Shimizu, K.-i.; Miyamoto, Y.; Kawasaki, T.; Tanji, T.; Tai, Y.; Satsuma, A. Chemoselective hydrogenation of nitroaromatics by supported gold catalysts: Mechanistic reasons of size- and support-dependent activity and selectivity. *J. Phys. Chem. C* **2009**, *113*, 17803–17810. [[CrossRef](#)]
60. Tan, Y.; Liu, X.Y.; Zhang, L.; Wang, A.; Li, L.; Pan, X.; Miao, S.; Haruta, M.; Wei, H.; Wang, H.; et al. ZnAl-hydrotalcite-supported Au₂₅ nanoclusters as precatalysts for chemoselective hydrogenation of 3-nitrostyrene. *Angew. Chem. Int. Ed.* **2017**, *56*, 2709–2713. [[CrossRef](#)]

61. Shimizu, K.-i.; Miyamoto, Y.; Satsuma, A. Size- and support-dependent silver cluster catalysis for chemoselective hydrogenation of nitroaromatics. *J. Catal.* **2010**, *270*, 86–94. [[CrossRef](#)]
62. Yoshida, H.; Kato, K.; Wang, J.; Meng, X.; Narisawa, S.; Fujita, S.I.; Wu, Z.; Zhao, F.; Arai, M. Hydrogenation of nitrostyrene with a Pt/TiO₂ catalyst in CO₂-dissolved expanded polar and nonpolar organic liquids: Their macroscopic and microscopic features. *J. Phys. Chem. C* **2011**, *115*, 2257–2267. [[CrossRef](#)]
63. Minejima, C.; Ebata, T.; Mikami, N. C-H stretching vibrations of benzene and toluene in their S1 states observed by double resonance vibrational spectroscopy in supersonic jets. *PCCP* **2002**, *4*, 1537–1541. [[CrossRef](#)]
64. Supriya, P.; Srinivas, B.T.V.; Chowdeswari, K.; Naidu, N.V.S.; Sreedhar, B. Biomimetic synthesis of gum acacia mediated Pd-ZnO and Pd-TiO₂-promising nanocatalysts for selective hydrogenation of nitroarenes. *Mater. Chem. Phys.* **2018**, *204*, 27–36. [[CrossRef](#)]
65. Nan, J.; Yu, H.B.; Xue, Q.S.; Li, Y.D. In situ FT-IR study on hydrogenation of olefin and aromatic on Pd-based metal catalysts. *Chem. Eng. Oil Gas* **2009**, *38*, 183–188.



© 2019 by the authors. Licensee MDPI, Basel, Switzerland. This article is an open access article distributed under the terms and conditions of the Creative Commons Attribution (CC BY) license (<http://creativecommons.org/licenses/by/4.0/>).